International Conference on Mathematics, Computational Methods & Reactor Physics (M&C 2009)
Saratoga Springs, New York, May 3-7, 2009, on CD-ROM, American Nuclear Society, LaGrange Park, IL (2009)

NUMERICAL INTEGRATION OF THE FEYNMAN PATH INTEGRAL FOR RADIATIVE TRANSPORT

Jerry Tessendorf
Rhythm and Hues Studios
5404 Jandy Place, Los Angeles, California 90066
jerryt@rhythm.com

ABSTRACT

The radiative transport problem is cast in integral form using a transport kernel. The transport kernel has an explicit representation in terms of a Feynman Path Integral over all paths between selected points in a volume. This representation is setup in detail. Numerical evaluation of this Path Integral is formulated with a Frenet-Serret based procedure for generating valid random paths, and with a numerical evaluation of the weight for each valid path. Very early sanity checks of a numerical implementation are reported. Approaches to optimization are identified.

Key Words: Radiative Transport, Feynman Path Integral, Monte Carlo, Frenet-Serret

1. INTRODUCTION

Radiative transport problems arise in many professional fields. A recent addition to this collection is computer graphics, and more specifically, visual effects production for feature films. In this field, radiative transport-based algorithms are usually limited to variations on single scattering of simple light sources illuminating clouds, smoke, water splashes, and gaseous phenomena that are purely artisticly motivated. There have been significant efforts to adopt better quality transport models, particularly including multiple scattering. Numerical integration methods like discrete ordinates are of little use in visual effects because ray affects would be too prominant. The Subsurface Scattering method [1] uses the diffusion approximation along with a well defined boundary and a uniform material within its shape. Photon Maps [2] have been extended to volumetric storage of distributions of raytraced light. And spherical harmonic methods [3] have been constructed, similar to Precomputed Radiance Transfer [4] for surface rendering. All of these methods have difficulty handling volumetric material with strong spatial variability, and/or high resolution visualization. The Monte Carlo path tracing method of Bouthors [5] achieves high resolution in the visualization. It uses statistical quantities based on random path tracing though a plane-parallel horizontally infinite slab of material. While it produces impressive imagery in some circumstances, it works best for relatively simple cauliflower- or stataform-like cloud shapes, and the applicability of plane-parallel calculations to complex shapes is uncertain.

The method discussed in this paper, direct numerical integration of a Feynman Path Integral solution for the radiative transport kernel, has several potential advantages. One of them is that very high angular and spatial resolution of the volume and visualization can be achieved. Also, the transport kernel can be introduced into the expression for the radiance in several different ways, so there are opportunities for keeping the existing volume rendering methods and incorporating multiple scattering as an additional effect. The potential downside of the Feynman

Path Integral evaluation is the high computational time. Even if it is prohibitively expensive in a production setting, numerial integration of the Feynman Path Integral will be a useful tool for further algorithm development.

2. RADIATIVE TRANSPORT KERNEL

In our optical application, the radiative transport equation handles absorption and scattering by the participating medium. The radiance distribution L at position $\mathbf{x}$ for light traveling in direction $\hat{\mathbf{n}}$ is governed by

$$\{\hat{\mathbf{n}} \cdot \nabla + c(\mathbf{x})\} \; L(\mathbf{x}, \hat{\mathbf{n}}) \; = \; b(\mathbf{x}) \int_{4\pi} d\Omega' \; P(\hat{\mathbf{n}}, \hat{\mathbf{n}}') \; L(\mathbf{x}, \hat{\mathbf{n}}') \; + \; S(\mathbf{x}, \hat{\mathbf{n}}) \tag{1}$$

The extinction coefficient $c = a + b$ is the sum of the scattering coefficient b and the absorption coefficient a. These coefficients are proportional to the density of the participating medium at any point in the volume, which varies from point to point via artistic construction. The term $S(\mathbf{x}, \hat{\mathbf{n}})$ is the source of light in the volume, and is typically one or more simple pointlights or spotlights. The phase function $P(\hat{\mathbf{n}}, \hat{\mathbf{n}}')$ is normalized to conserve energy:

$$\int_{4\pi} d\Omega \; P(\hat{\mathbf{n}}, \hat{\mathbf{n}}') \; = \; \int_{4\pi} d\Omega' \; P(\hat{\mathbf{n}}, \hat{\mathbf{n}}') \; = \; 1 \tag{2}$$

In our typical usage we consider the phase function to be independent of position within the volume (although this assumption could be removed in the Path Integral formulation), and homogeneous in directions, meaning that it's dependence on the incoming and outgoing directions depends only on the angle between them, i.e. only on their inner product. Examples of these conditions, within useful approximation, include many types of droplet clouds, smoke, liquid water, and organic tissue. Consequently we can label the angular dependence of the phase function as

$$P(\hat{\mathbf{n}}, \hat{\mathbf{n}}') \;\; \text{or} \;\; P(\hat{\mathbf{n}} \cdot \hat{\mathbf{n}}') \;\; \text{or} \;\; P(|\hat{\mathbf{n}} - \hat{\mathbf{n}}'|) \tag{3}$$

It is also useful to express the phase function in terms of a Fourier-like integral,

$$P(\hat{\mathbf{n}} \cdot \hat{\mathbf{n}}') \; = \; \int \frac{d^3p}{(2\pi)^3} \; \tilde{Z}(|\mathbf{p}|) \exp\left(\mathbf{p} \cdot (\hat{\mathbf{n}} - \hat{\mathbf{n}}')\right) \tag{4}$$

The amplitude $\tilde{Z}$ is a function of the magnitude of the vector $\mathbf{p}$ because the phase function only depends on $\hat{\mathbf{n}} \cdot \hat{\mathbf{n}}'$. Note that the amplitude $\tilde{Z}$ cannot be obtained by an inverse Fourier transform, because the phase function is defined only on the disk $|\hat{\mathbf{n}} - \hat{\mathbf{n}}'| \leq 2$, and not over all of R^3 as would be required to perform the transform. Nevertheless, this Fourier expression for the phase function is useful because the inverse transform is never needed to obtain the Path Integral representation.

To generate an explicit solution for this equation, we reformulate it as a time-dependent problem, then introduce a kernel for the homogeneous equation. The time-dependence in this approach is not a physical interpretation of time, just a convenient reparameterization. The transport equation is this instance is

$$\left\{ \frac{\partial}{\partial s} + \hat{\mathbf{n}} \cdot \nabla + c(\mathbf{x}) \right\} \; L(s, \mathbf{x}, \hat{\mathbf{n}}) \; = \; b(\mathbf{x}) \int_{4\pi} d\Omega' \; P(\hat{\mathbf{n}}, \hat{\mathbf{n}}') \; L(s, \mathbf{x}, \hat{\mathbf{n}}') \; + \; S(\mathbf{x}, \hat{\mathbf{n}}) \tag{5}$$

where s is the artificial time variable times the speed of light (and has units of length). The kernel for the homogeneous case satisfies the unsourced transport equation and an initial condition:

$$\left\{ \frac{\partial}{\partial s} + \hat{\mathbf{n}} \cdot \nabla + c(\mathbf{x}) \right\} G(s, \mathbf{x}, \hat{\mathbf{n}}, \mathbf{x}', \hat{\mathbf{n}}') = b(\mathbf{x}) \int_{4\pi} d\Omega'' \, P(\hat{\mathbf{n}}, \hat{\mathbf{n}}'') \, G(s, \mathbf{x}, \hat{\mathbf{n}}'', \mathbf{x}', \hat{\mathbf{n}}') \quad (6)$$

$$G(s = 0, \mathbf{x}, \hat{\mathbf{n}}, \mathbf{x}', \hat{\mathbf{n}}') = \delta(\mathbf{x} - \mathbf{x}') \, \delta(\hat{\mathbf{n}} - \hat{\mathbf{n}}') \quad (7)$$

The explicit solution of equation 1 for the radiance is

$$L(\mathbf{x}, \hat{\mathbf{n}}) = \int_0^\infty ds \int d^3x' \int_{4\pi} d\Omega' \, G(s, \mathbf{x}, \hat{\mathbf{n}}, \mathbf{x}', \hat{\mathbf{n}}') \, S(\mathbf{x}', \hat{\mathbf{n}}') \quad (8)$$

This equation is the conceptual basis of current approaches to volume rendering in film production, though actual implementations are highly simplified ray marchs that only incorporate single scattering. An improved calculation of the kernel G would better reproduce multiple scattering physics.

3. FEYNMAN PATH INTEGRAL FOR THE KERNEL

The transport kernel G has an explicit representation in terms of Feynman Path Integrals. The first version of this was published without time-dependence[6], and suffered from an inability to handle backscattering. This limitation originated in the framing of the problem, not in the Path Integral approach. Subsequent refinement and expansion to the time-dependent form in [7] and [8][12] eliminated this problem while also simplifying the structure of the Path Integral. A brief derivation is provided in the appendix below.

In the Path Integral representation of G, paths of length s through the volume are described by positions along a curve, $\mathbf{x}(s'),\ 0 \leq s' \leq s$, and by their unit tangent vectors

$$\hat{\beta}(s') = \frac{d\mathbf{x}(s')}{ds'} \quad (9)$$

along the curve. The time parameter takes on the role of the arclength for parameterized paths. The paths of interest for evaluating G are the ones that start at $\mathbf{x}'$ traveling in direction $\hat{\mathbf{n}}'$, end at position $\mathbf{x}$ and direction $\hat{\mathbf{n}}$, and have a total arclength of s. The Path Integral can only include paths which individually satisfy the constraints

$$\hat{\beta}(0) = \hat{\mathbf{n}}' \quad \hat{\beta}(s) = \hat{\mathbf{n}} \quad (10)$$

$$\mathbf{x} - \mathbf{x}' = \int_0^s ds' \, \hat{\beta}(s') \quad (11)$$

Each path is assigned a weight for its contribution to the kernel. Physically this weight depends on the distribution of material that the path encounters, and the amount of scattering that alters the direction of the path. Intuitively, changes of path direction are characterized by changes of the path tangent vector $\hat{\beta}$, so we can expect that the path weight depends on a combination of $d\hat{\beta}/ds'$, the phase function, and the scattering coefficient $b(\mathbf{x})$. More specifically, the phase function

behavior in equation 4 means that the dependence on $d\hat{\beta}/ds'$ is only on it's magnitude, $|d\hat{\beta}/ds'|$, which is the intrinsic curvature κ defined in the Frenet-Serret representation of space curves.

Following the appendix below, the Path Integral representation for the kernel is

$$\begin{aligned} G(s,\mathbf{x},\hat{\mathbf{n}},\mathbf{x}',\hat{\mathbf{n}}') &= \int \prod_{s'} d\Omega_{\hat{\beta}}(s') \prod_{s'} d^3p(s') \;\; \delta(\hat{\beta}(0)-\hat{\mathbf{n}}')\,\delta(\hat{\beta}(s)-\hat{\mathbf{n}}) \\ &\times \;\; \delta\left(\mathbf{x}-\mathbf{x}'-\int_0^s ds'\;\hat{\beta}(s')\right) \\ &\times \;\; \exp\left(-\int_0^s ds'\;c(\mathbf{x}(s'))\right)\;\exp\left(i\int_0^s ds'\;\mathbf{p}(s')\cdot\frac{d\hat{\beta}(s')}{ds'}\right) \\ &\times \;\; \exp\left(\int_0^s ds'\;b(\mathbf{x}(s'))\;\tilde{Z}(|\mathbf{p}(s')|)\right) \end{aligned} \tag{12}$$

This Path Integral has three main components: (1) The integration measure $\prod_{s'} d\Omega_{\hat{\beta}}(s')$ runs over all possible curve shapes by using the curve tangents as the integration variable; (2) The delta functions constrain the contributing curves to only those that meet the conditions in equations 10-11; (3)The remaining factors are the weight for each path.

There have been multiple approaches to approximately evaluating this Path Integral for the transport kernel, based on steepest-descents and WKB types of approximations. While they produce better understanding of the transport problem [8][9][10], they have proven insufficient for high quality approximations to multiple scattering. In the next section we establish a plan for numerically evaluating this Path Integral, then discuss some of the details of implementation.

4. NUMERICAL SCHEME FOR INTEGRATION

The numerical scheme described here is a deconstruction of the Path Integral into a discrete representation for all of the factors in it. There are three basic components of interest, the first two of which are presented in detail in sections 4.1 and 4.2. The third is the subject of future work.

1. Establish a discrete representation of paths through the volume, which are guaranteed to satisfy the constraints in equations 10-11. We have chosen for this a discretization of Frenet-Serret paths, combined with a procedure for modifying those paths while enforcing the constraints. Section 4.1 provides detail. This approach lends itself to a Monte Carlo process for sampling many paths in the volume by successive deformations.
2. On each segment of a discrete path, weights are assigned based on the Path Integral integrand. In order to do this numerically, we regularize the integrand. The regularization has the effect of broadening the forward scattering peak of the phase function, and in practice the broadening can be made much smaller than the physical width of common materials of interest. This is discussed in detail in section 4.2
3. With the ability to generate random paths and weight each one, we need a procedure to efficiently capture the most important paths for any given configuration of the participating

medium. This is a critically important topic for practical calculations, but is not address in this paper.

4.1. Generating Constrained Frenet-Serret Paths

The constraints in the Path Integral can be broken down into a set of five criteria for the paths that we construct for the numerical evaluation:

C1 The paths originate at the point $\mathbf{x}'$.

C2 The tangent vectors at the origination point are $\hat{\mathbf{n}}'$.

C3 The paths have fixed length s.

C4 The paths terminate at the point $\mathbf{x}$.

C5 The tangent vectors at the terminal point are $\hat{\mathbf{n}}$.

We have chosen to represent the paths in the Path Integral using curves defined in the Frenet-Serret framework. The advantage of doing this is that requirements C1-C3 are satisfied by Frenet-Serret curves. We will satisfy criteria C4 and C5 by starting with a simple curve satisfying all of the criteria, then systematically deform it at multiple points using criteria C4 and C5 as constraints on the deformation. The process of constrained deformation of discrete Frenet-Serret curves in described in section 4.1.3, after showing a discrete version of the Frenet-Serret framework in section 4.1.2.

4.1.1. Frenet-Serret Space Curves

The Frenet-Serret framework describes arbitrary curves in space in terms of the intrinsic curvature κ and torsion τ at every point along the curve [11]. At each point of the curve there is a framework $\{\hat{\mathbf{T}}, \hat{\mathbf{N}}, \hat{\mathbf{B}}, \kappa, \tau\}$, in which $\hat{\mathbf{T}}$, $\hat{\mathbf{N}}$, and $\hat{\mathbf{B}}$ are an orthonormal local coordinate system, with $\hat{\mathbf{T}}$ being the tangent to the curve. For our Path Integral application, this tangent vector is the same as the tangent vector integration variable $\hat{\beta}$ in equation 12.

If $\mathbf{x}(s')$ is a space curve parameterized by arclength s', then the framework satisfies the equations

$$\frac{d\mathbf{x}(s')}{ds'} = \hat{\mathbf{T}}(s') \tag{13}$$

$$\frac{d\hat{\mathbf{T}}(s')}{ds'} = \kappa(s')\,\hat{\mathbf{N}}(s') \tag{14}$$

$$\frac{d\hat{\mathbf{N}}(s')}{ds'} = -\kappa(s')\,\hat{\mathbf{T}}(s') + \tau(s')\,\hat{\mathbf{B}}(s') \tag{15}$$

$$\frac{d\hat{\mathbf{B}}(s')}{ds'} = -\tau(s')\,\hat{\mathbf{N}}(s') \tag{16}$$

Note that these equations have a compact form, using a quantity $\vec{\mathbf{F}}(s')$ that is a triplet of the

orthonormal basis vectors:

$$\vec{\mathbf{F}}(s') \equiv \begin{pmatrix} \hat{\mathbf{T}}(s') \\ \hat{\mathbf{N}}(s') \\ \hat{\mathbf{B}}(s') \end{pmatrix} \tag{17}$$

Then the equations 14-16 for the basis can be written more compactly as

$$\frac{d\vec{\mathbf{F}}(s')}{ds'} = A(s')\,\vec{\mathbf{F}}(s') \tag{18}$$

where A is a 3×3 matrix

$$A(s') = \begin{bmatrix} 0 & \kappa(s') & 0 \\ -\kappa(s') & 0 & \tau(s') \\ 0 & -\tau(s') & 0 \end{bmatrix} \tag{19}$$

which mixes the orthonormal basis. This equation also shows that curves can be constructed from the knowledge of only the curvature and torsion at every point of the curve, the position of the root of the curve, and the orientation at the root. The curve can be deformed by altering the values of κ and τ at any point on the curve.

4.1.2. Discrete Curves

For the discrete form of the Frenet-Serret representation, we choose a finite segment length Δs between discrete nodes along the length of a curve. A curve consists of the root position $\mathbf{x}_0$ and basis $\vec{\mathbf{F}}_0 = (\hat{\mathbf{T}}_0, \hat{\mathbf{N}}_0, \hat{\mathbf{B}}_0)$, and the values of curvature and torsion $(\kappa_i, \tau_i),\ i = 0 \ldots N-1$ at each node along the curve. Within each segment, the curvature and torsion are constant, so equation 18 can be integrated to give the transition from node to node

$$\vec{\mathbf{F}}_{i+1} = U_i\,\vec{\mathbf{F}}_i \tag{20}$$

where the 3×3 matrix U_i is

$$\begin{aligned} U_i &= \exp\left(A_i\,\Delta s\right) \\ &= \begin{bmatrix} 1 - \frac{\kappa_i^2}{\ell^2}\left(1 - \cos(\ell\,\Delta s)\right) & \frac{\kappa_i}{\ell}\sin(\ell\,\Delta s) & \frac{\kappa_i\,\tau_i}{\ell^2}\left(1 - \cos(\ell\,\Delta s)\right) \\ -\frac{\kappa_i}{\ell}\sin(\ell\,\Delta s) & \cos(\ell\,\Delta s) & \frac{\tau_i}{\ell}\sin(\ell\,\Delta s) \\ \frac{\kappa_i\,\tau_i}{\ell^2}\left(1 - \cos(\ell\,\Delta s)\right) & -\frac{\tau_i}{\ell}\sin(\ell\,\Delta s) & 1 - \frac{\tau_i^2}{\ell^2}\left(1 - \cos(\ell\,\Delta s)\right) \end{bmatrix} \end{aligned} \tag{21}$$

and $\ell = \sqrt{\kappa_i^2 + \tau_i^2}$.

Also, the integral form of equation 13 gives the position of each node as

$$\mathbf{x}_i = \mathbf{x}_0 + \sum_{j=0}^{j<i} \hat{\mathbf{T}}_j\,\Delta s \tag{22}$$

4.1.3. Constrained Deformation

This discrete form of the Frenet-Serret representation generates arbitrary curves by choosing different values for (κ, τ) at each node. If we start with a discrete curve which satisfies constraints C1-C5, and replace (κ_i, τ_i) at one node i, then the new curve still satisfies constraints C1-C3, but in general can violate C4 and C5. These last two constraints can be restored by modifying the curve at two more nodes. Intuitively, changing the values at one node changes the position and direction at the final node. Adding coordinated changes at two other nodes restores the position and direction constraints. The specific procedure described below generates curves by successive constrained deformation of an input curve:

1. Choose three nodes i_0, i_1, i_2, ($i_0 < i_1 < i_2$) at which the deformation is to be applied.
2. Change the value of the curvature κ_{i_1} at the middle node to a new desired value.
3. Use a newton root solver to find new values of κ_{i_0}, κ_{i_2}, τ_{i_0}, τ_{i_1}, τ_{i_2} which preserve constraints C4 and C5.

The root solver typically take 2-10 iterations to arrive at a reasonable result. Occasionally some choices of κ_{i_1} will not satisfy constraints C4 and C5, and the root solver will not converge. For efficiently, we discard a value of κ_{i_1} if the solver has not converged after 20 iterations.

4.2. Path Weighting

For each path generated as in section 4.1.3, the Path Integral assigns a corresponding weight, which is the product of weights occuring at each node of the path. The weight at node n is

$$\omega_n = e^{-c_n \Delta s} \int \frac{d^3 p}{(2\pi)^3} \exp\left(i\mathbf{p} \cdot \hat{\mathbf{N}}_n \, \kappa_n \Delta s \; + \; b_n \Delta s \tilde{Z}(|\mathbf{p}|) \right) \tag{23}$$

where c_n and b_n are the optical properties at the location of the node. The full contribution of a path to the Path Integral is

$$\omega_{path} = \prod_{n=0}^{N-1} \omega_n \tag{24}$$

Note that the solid angle portion of the integral can be performed exactly because $\tilde{Z}$ depends only on the magnitude of $\mathbf{p}$. Using spherical coordinates, the integral becomes

$$\omega_n = e^{-c_n \Delta s} \int_0^\infty \frac{dp}{2\pi^2} \, p^2 \, J_0\left(p \kappa_n \Delta s\right) \, \exp\left(b_n \Delta s \tilde{Z}(p) \right) \tag{25}$$

This integral is difficult to evaluate numerically because it convergences only in the distributional sense: even though $\tilde{Z} \to 0$ as $p \to \infty$, the integrand does not go to zero. In fact, the case $\tilde{Z} = 0$ gives a Dirac delta function, which enforces no scattering. One approach to make this a numerically tractable integral is to explicitly extract the delta function portion, rewriting ω_n as

$$\omega_n = e^{-c_n \Delta s} \delta(\hat{\mathbf{N}}_n \kappa_n \Delta s) + e^{-c_n \Delta s} \int_0^\infty \frac{dp}{2\pi^2} \, p^2 \, J_0\left(p \kappa_n \Delta s\right) \, \left(\exp\left(b_n \Delta s \tilde{Z}(p) \right) \; - \; 1 \right) \tag{26}$$

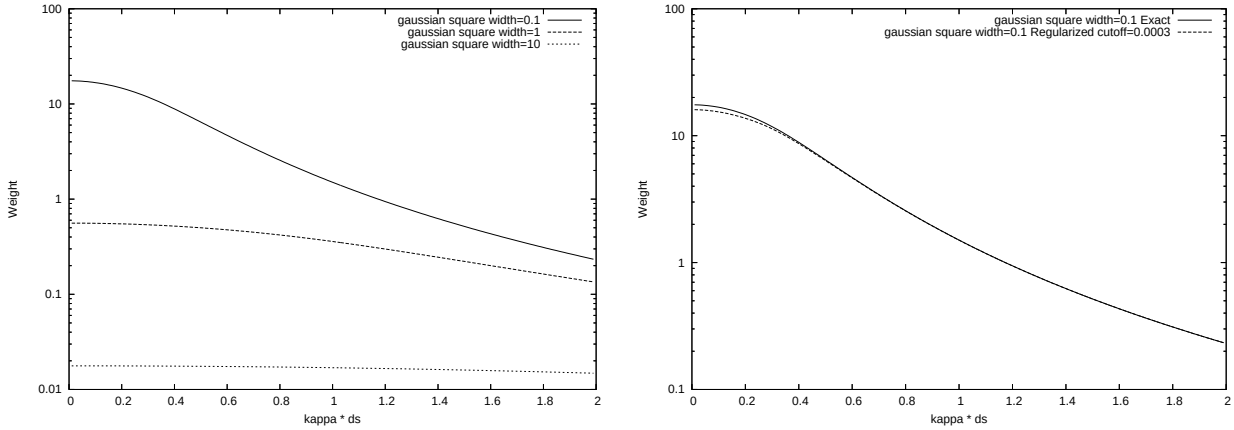

Figure 1. *Left:* Path Integral weight as a function of $\kappa\Delta s$, for $b\Delta s = 1$. A gaussian phase function is used. Each curve is a different value of the width of the phase function. The width values, from top to bottom, are 0.1, 1.0, and 10.0. *Right:* Path Integral weight computed using a regularization of the integral instead of separating the no-scatter delta function, compared with directly removing the Dirac delta function from the integrand.

This integrand is numerically well-behaved. The plot on the left in Figure 1 illustrates the non-delta function part of the weight as a function of $\kappa\Delta s$ for $b\Delta s = 1.0$. For this example, we chose a gaussian phase function, for which $\tilde{Z}$ is also gaussian. The three curves correspond to different values of the square width of the gaussian. Although this provides a way of accurately evaluating the scattering portion of the weight, it is still difficult to handle the delta function term in equation 26 in a numerical setting.

A second method of computing the path weighting, which better handles the non-scattering delta function, is to regularized the integrand. In this situation, equation 25 is modified to

$$\omega_n^R = e^{-c_n \Delta s} \int_0^\infty \frac{dp}{2\pi^2}\, p^2\, J_0\left(p\kappa_n \Delta s\right)\, \exp\left(b_n \Delta s \tilde{Z}(p) - \frac{\epsilon}{2} p^2\right) \tag{27}$$

The additional term includes a regularization parameter ϵ, and in the limit the $\epsilon \to 0$, $\omega_n^R \to \omega_n$. However, for $\epsilon \neq 0$, the integral is well-behaved numerically. The plot on the right of Figure 1 compares the previous method and the regularized weight, for $\epsilon = 0.0003$. This method also handles the unscattered case reasonably, because when $\tilde{Z} = 0$, the integrand is a standard distributional definition of the Dirac delta function. Regulatization in this fashion has the effect of broadening the peak of the weights a small amount proportional to $\epsilon^{1/2}$.

5. PRELIMINARY CALCULATIONS

The numerical procedures outlined in section 4 have been implemented recently in C++. The code is currently in a verification stage. The code executes under MPI by distributing from a primary node to each MPI node the task of generating many random paths between $(\mathbf{x}', \hat{\mathbf{n}}')$ and $(\mathbf{x}, \hat{\mathbf{n}})$, computing the weight of each path, and summing all of the weights for the paths

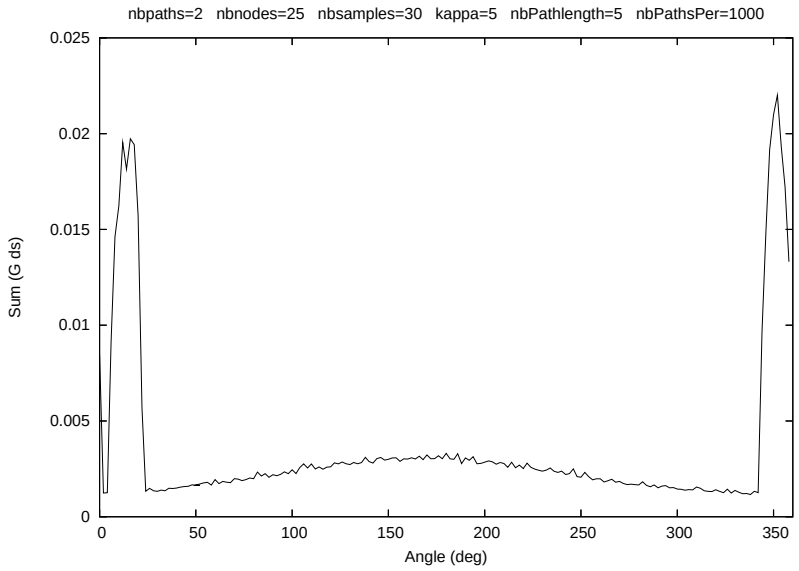

Figure 2. Preliminary calculation of the integral of the transport kernel over pathlength, as a function of the angle between incoming and outgoing directions. The number and distribution of paths used in this calculation is insufficient for quantitative use of this result. This data serves only for code verification procedures.

computed. This sum is returned to the primary node for assimilation with the results of other nodes. Each MPI node receives additional work generating paths and weights immediately after finishing the previous one. The cluster is a mixture of AMD and Intel machines of several generations, all operating under a variant of SuSe 9.2 Linux. The cluster normally functions as a queue-based image render farm for visual effects production, with MPI running independent of the queue. Depending on the production rendering load, between 10 and 3000 nodes are available for MPI. Figure 2 is a very preliminary example of calculations performed with this code for the quantity $\int_0^\infty ds\ G(s, \mathbf{x}, \hat{\mathbf{n}}, \mathbf{x}', \hat{\mathbf{n}}')$ as a function of the angle between $\hat{\mathbf{n}}$ and $\hat{\mathbf{n}}'$. This figure represents only very preliminary verification calculations and so no scientific, engineering, or artistic insights can be drawn from them. The peaks are near the direct line between $\mathbf{x}$ and $\mathbf{x}'$, and the minimum near 2 degrees probably indicates that there is an insufficient sampling paths and path fluctuations near the direct line in this calculation for an accurate result.

6. CONCLUSIONS

The Path Integral formulation of radiative transport shows promise as a method of directly computing the transport kernel. In this paper a numerical scheme is outlined for direct numerical integration of the Path Integral, and a preliminary implementation of a code discussed. The code uses Monte Carlo procedures to generate valid paths satisfying the constraints imposed by the transport kernel. Using a discrete Frenet-Serret representation of the paths, a small set of constraints are satisfied via a newton root finding scheme which converges typically in 2-10 iterations. A numerical weight is computed for each valid path, based on the scattering function, optical properties, and the Frenet-Serret curvature of the path.

There are a number of optimizations planned for the present code. For example, the smooth character of the curves in Figure 1 shows that it is feasible to store the weights in a lookup table instead of calculating the integral numerically each time. We intend to incorporate importance sampling for the path generation. We also plan a number of sensitivity studies for variation of parameters, e.g. the number of path segments, number of deformations of a path, total number of paths, length of path segments, and more.

REFERENCES

[1] Henrik Wann Jensen, Steve Marschner, Marc Levoy, and Pat Hanrahan, "A Practical Model for Subsurface Light Transport," *Proceedings of SIGGRAPH 2001*, pp. 511-518, Los Angeles, August 2001.

[2] Henrik Wann Jensen and Per H. Christensen, "Efficient Simulation of Light Transport in Scenes with Participating Media using Photon Maps," *Proceedings of SIGGRAPH 1998*, pp. 311-320, Orlando, July 1998.

[3] Nafees Bin Zafar, Johan Akesson, Doug Roble, and Ken Museth, "Scattered spherical harmonic approximation for accelerated volume rendering," *International Conference on Computer Graphics and Interactive Techniques, ACM SIGGRAPH 2006 Sketches*, (2006).

[4] Peter-Pike Sloan, Jan Kautz, and John Snyder. "Precomputed Radiance Transfer for Real-Time Rendering in Dynamic, Low-Frequency Lighting Environments". *ACM Transactions on Graphics, Proceedings of the 29th Annual Conference on Computer Graphics and Interactive Techniques (SIGGRAPH)*, pp. 527-536. New York, NY: ACM Press, 2002.

[5] Antoine Bouthors, Fabrice Neyret, Nelson Max, Eric Bruneton, Cyril Crassin, "Interactive multiple anisotropic scattering in clouds," *ACM Symposium on Interactive 3D Graphics and Games (I3D) - 2008*, (2008).

[6] J. Tessendorf, "Radiative Transfer as a Sum over Paths," *Physical Review A*, **35**, no. 2, pp. 872-878 (1987).

[7] J. Tessendorf, "Time Dependent Radiative Transfer and Pulse Evolution" *J. Opt. Soc. Am. A*, **6**, no. 2, pp. 280-297 (1989).

[8] Lev T. Perelman, Jun Wu, Irving Itzkan, and Michael S. Feld, "Photon Migration in Turbid Media Using Path Integrals," *Phys. Rev. Lett.*, **72**, pp. 1341-1344, (1994).

[9] Simon Premoze, Michael Ashikhmin, Jerry Tessendorf, Ravi Ramamoorthi, and Shree Nayar, "Practical Rendering of Multiple Scattering Effects in Participating Media," *Eurographics Symposium on Rendering*, (2004).

[10] J. Tessendorf and D. Wasson, "Impact of Multiple Scattering on Simulated Infrared Cloud Scene Images,", *Characterization and Propagation of Sources and Backgrounds*, SPIE Publication **2223**, pp. 462-473 (1994)

[11] Millman and Parker, *Elements of Differential Geometry*, Prentice-Hall, (1977).

[12] S. D. Miller, "Stochastic construction of a Feynman path integral representation for Green's functions in radiative transfer," *J. Math. Physics*, **39**, Issue 10, pp. 5307-5315 (1998)

APPENDIX: PATH INTEGRAL CONSTRUCTION

Here we construct the Path Integral representation of the transport kernel. To simplify the presentation, the extinction coefficients c and b are assumed to be spatially uniform. When they vary from point to point in the volume, the construction below can be reworked to arrive at the result shown in equation 12.

A basic property of the transport kernel is that it can be decomposed into the action of two kernels. Physically, this says that transport over a period of time s can be decomposed into transport over two successive time periods s_0 and s_1, with $s = s_0 + s_1$. Mathematically this is the convolution of two kernels over the two time intervals:

$$G(s, \mathbf{x}, \hat{\mathbf{n}}, \mathbf{x}', \hat{\mathbf{n}}') = \int d^3x_1 \, d\Omega_1 \, G(s_1, \mathbf{x}, \hat{\mathbf{n}}, \mathbf{x}_1, \hat{\mathbf{n}}_1) \, G(s_0, \mathbf{x}_1, \hat{\mathbf{n}}_1, \mathbf{x}', \hat{\mathbf{n}}') \tag{28}$$

Of course, we can continue this decomposition and divide the total time into many intervals. The full kernel is a succession of convolutions of kernels for the N intervals:

$$G(s, \mathbf{x}, \hat{\mathbf{n}}, \mathbf{x}', \hat{\mathbf{n}}') = \int \prod_{i=1}^{N-1} d^3x_i \, d\Omega_i \; \prod_{i=1}^{N} G(\Delta s, \mathbf{x}_i, \hat{\mathbf{n}}_i, \mathbf{x}_{i-1}, \hat{\mathbf{n}}_{i-1}) \tag{29}$$

where Δs is the amount of time in each interval ($s = N\Delta s$), $(\mathbf{x}_0, \hat{\mathbf{n}}_0) = (\mathbf{x}', \hat{\mathbf{n}}')$ and $(\mathbf{x}_N, \hat{\mathbf{n}}_N) = (\mathbf{x}, \hat{\mathbf{n}})$.

To obtain the Path Integral, we will seek to subdivide the interval into infinitely many infinitismal intervals, i.e. take the limit $N \to \infty$, $\Delta s \to 0$ such that s remains fixed. In that limit, Δs is very small, so we can express the transport kernel in each interval as a single scattering result:

$$G(\Delta s, \mathbf{x}_i, \hat{\mathbf{n}}_i, \mathbf{x}_{i-1}, \hat{\mathbf{n}}_{i-1}) = e^{-c\Delta s} \delta\left(\mathbf{x}_i - \mathbf{x}_{i-1} - \hat{\mathbf{n}}_i \Delta s\right) \left[\delta\left(\hat{\mathbf{n}}_i - \hat{\mathbf{n}}_{i-1}\right) \; + b\Delta s P(\hat{\mathbf{n}}_i, \hat{\mathbf{n}}_{i-1})\right] \tag{30}$$

To be able to take the limit $\Delta s \to 0$ with $N \to \infty$, we will need a way of representing the second factor with the angular dependence in a more friendly way. We can accomplish this using the Fourier representation. When the phase function $P(\hat{\mathbf{n}}, \hat{\mathbf{n}}')$ depends only on the inner product $\hat{\mathbf{n}} \cdot \hat{\mathbf{n}}'$, then it can be expanded in Fourier modes as

$$P(\hat{\mathbf{n}}, \hat{\mathbf{n}}') = \int \frac{d^3p}{(2\pi)^3} \tilde{Z}(|\mathbf{p}|) \; \exp\left(i\mathbf{p} \cdot (\hat{\mathbf{n}} - \hat{\mathbf{n}}')\right) \tag{31}$$

The case when the phase function does not have this symmetry was considered in [6]. Exploiting this Fourier Transform representation, and the fact that $b\Delta s$ becomes arbitrarily small in the final limit, the angular factor becomes

$$\delta\left(\hat{\mathbf{n}}_i - \hat{\mathbf{n}}_{i-1}\right) \; + b\Delta s P(\hat{\mathbf{n}}_i, \hat{\mathbf{n}}_{i-1}) = \int \frac{d^3p}{(2\pi)^3} \; \exp\left(i\mathbf{p} \cdot (\hat{\mathbf{n}}_i - \hat{\mathbf{n}}_{i-1})\right) \; \exp\left(b\Delta s \tilde{Z}(|\mathbf{p}|)\right) \tag{32}$$

This expression also allows us to put together all of the intervals and group the factors in a fairly compact way:

$$\begin{aligned} G(s, \mathbf{x}, \hat{\mathbf{n}}, \mathbf{x}', \hat{\mathbf{n}}') \;\; &= \;\; e^{-cs} \int \prod_{i=1}^{N-1} d\Omega_i \, \frac{d^3p_i}{(2\pi)^3} \; \exp\left(i \sum_{i=1}^{N} \mathbf{p}_i \cdot (\hat{\mathbf{n}}_i - \hat{\mathbf{n}}_{i-1})\right) \; \exp\left(\sum_{i=1}^{N} b\Delta s \tilde{Z}(|\mathbf{p}_i|)\right) \\ &\times \;\; \int \prod_{i=1}^{N-1} d^3x_i \; \prod_{i=1}^{N} \delta\left(\mathbf{x}_i - \mathbf{x}_{i-1} - \hat{\mathbf{n}}_i \Delta s\right) \end{aligned}$$

At this stage the spatial integrals can be evaluated exactly because they are a nested sequence of delta functions. Explicity, they evaluate to

$$\int \prod_{i=1}^{N-1} d^3x_i \prod_{i=1}^{N} \delta\left(\mathbf{x}_i - \mathbf{x}_{i-1} - \hat{\mathbf{n}}_i \Delta s\right) = \delta\left(\mathbf{x}_N - \mathbf{x}_0 - \sum_{i=1}^{N} \hat{\mathbf{n}}_i \, \Delta s\right) \tag{33}$$

This sequence of substitutions and decompositions leaves us in good condition to take the continuum limit $\Delta s \to 0$, $N \to \infty$. In this limit, the sums in the various terms become integrals. If we identify the continuous unit vector valued function $\hat{\beta}(s')$ with the direction vectors by $\hat{\beta}(s' = i\Delta s) = \hat{\mathbf{n}}_i$, then the spatial delta function becomes in the continuum limit:

$$\delta\left(\mathbf{x}_N - \mathbf{x}_0 - \sum_{i=1}^{N} \hat{\mathbf{n}}_i \, \Delta s\right) \;\to\; \delta\left(\mathbf{x} - \mathbf{x}' - \int_0^s \hat{\beta}(s') \, ds'\right) \tag{34}$$

Similarly, the factor containing the Fourier modes $\tilde{Z}$ of the phase function becomes an integral in the limit

$$\exp\left(\sum_{i=1}^{N} b\Delta s \tilde{Z}(|\mathbf{p}_i|)\right) \;\to\; \exp\left(\int_0^s b\tilde{Z}(|\mathbf{p}(s')|)ds'\right) \tag{35}$$

The last factor to convert to the continuum limit is the sum of the Fourier phase terms. By multiplying and dividing simultaneously by Δs, we can recognize that

$$\frac{\hat{\mathbf{n}}_i - \hat{\mathbf{n}}_{i-1}}{\Delta s}$$

is a finite difference version of a derivative, and so in the continuum limit it becomes $d\hat{\beta}(s')/ds'$ and the full factor is

$$i\sum_{i=1}^{N-1} \mathbf{p}_i \cdot (\hat{\mathbf{n}}_i - \hat{\mathbf{n}}_{i-1}) = i\sum_{i=1}^{N-1} \mathbf{p}_i \cdot \frac{(\hat{\mathbf{n}}_i - \hat{\mathbf{n}}_{i-1})}{\Delta s}\Delta s \;\to\; i\int_0^s \mathbf{p}(s') \cdot \frac{d\hat{\beta}(s')}{ds'} ds' \tag{36}$$

Assembling all of these results for limits, the final Path Integral expression for the transport kernel is

$$\begin{aligned} G(s, \mathbf{x}, \hat{\mathbf{n}}, \mathbf{x}', \hat{\mathbf{n}}') &= e^{-cs} \int d\mu \, \delta\left(\hat{\beta}(0) - \hat{\mathbf{n}}'\right) \, \delta\left(\hat{\beta}(s) - \hat{\mathbf{n}}\right) \, \delta\left(\mathbf{x} - \mathbf{x}' - \int_0^s \hat{\beta}(s')ds'\right) \\ &\times \exp\left(i\int_0^s \mathbf{p}(s') \cdot \frac{d\hat{\beta}(s')}{ds'} ds'\right) \exp\left(\int_0^s b\tilde{Z}(|\mathbf{p}(s')|)ds'\right) \end{aligned}$$

We have also inserted delta function factors $\delta\left(\hat{\beta}(0) - \hat{\mathbf{n}}'\right) \, \delta\left(\hat{\beta}(s) - \hat{\mathbf{n}}\right)$ in order to explicitly enforce the "boundary conditions" imposed early that the tangent of the path has fixed values at the beginning and end of the path. Also, the integration measure $d\mu$ is the "continuum limit" of the discreet multidimensional measure $\prod_i d\Omega_i \, d^3p_i/(2\pi)^3$.